International Journal of Heat and Technology
Vol. 44, No. 3, June, 2026, pp. 976-986
Journal homepage: http://iieta.org/journals/ijht

Influence of Edge Number of Vortex Generators on Thermo-Hydraulic Performance of Compact Heat Exchangers

Ayad Ali Mohammed*, Haider Fawzi Mahmood

Al-Mussaib Technical College, Al-Furat Al-Awsat Technical University, Babylon 51006, Iraq

Corresponding Author Email: ayadia1@atu.edu.iq

https://doi.org/10.18280/ijht.440307

Received: 13 April 2026
Revised: 4 June 2026
Accepted: 17 June 2026
Available online: 30 June 2026

Keywords:
vortex generators, compact heat exchanger, edge number, thermo-hydraulic performance, Computational Fluid Dynamics, Nusselt number, entropy generation, field synergy principle

ABSTRACT

This study investigated the effect of the number of vortex generator (VG) edges on the thermo-hydraulic characteristics of a rectangular compact heat exchanger. A coupled approach was used for the investigation, where Reynolds number (Re) ranged from 1000–5000. In this study, five different block-type VG with different edge numbers, N = 3, 4, 5, 6, and ∞, were used. The VGs had the same frontal area, height, and angle of attack for a fair comparison. The results showed that the heat transfer performance was improved for all VGs compared to the smooth channel. The best heat transfer performance was achieved using a pentagonal VG. The performance evaluation criterion (PEC) was approximately 1.56 at Re = 5000. The friction penalty increased with the sharpness of the VGs. The smoother the VGs, the lower the thermal enhancement was. The study showed that the heat transfer performance improved for all the VGs. The coupled approach was validated using a data-driven method. The PEC was a function of Re and the edge number. The results highlighted that the edge number is a practical parameter for enhancing the performance of compact heat exchangers.

1. INTRODUCTION

Compact heat exchangers (CHEs) play an important role in current thermal systems, such as car radiators, aircraft cooling, heating, ventilation, air conditioning, and electronic thermal management systems. The small volume and high surface area per unit volume of CHEs make them highly efficient; however, increasing heat rejection in limited spaces has led to the need for innovative heat transfer enhancement technologies [1, 2].

Heat transfer enhancement techniques are generally divided into two classes: active and passive. Passive methods, on the other hand, have many advantages over active methods in that they are simple, reliable, and do not require external energy sources. An effective method for passive heat transfer enhancement is the use of vortex generators (VGs), which create secondary flow fields in a fluid by generating longitudinal vortices [2-4].

Although various VG geometries have been investigated in previous studies, most analyses remain geometry specific. This study introduces an edge-number-based parameterization method to enable consistent comparisons across polygonal vortex configurations. Previous studies have demonstrated that VGs can increase the Nusselt number (Nu) by 20–60%, depending on their geometry and placement, although this enhancement is typically accompanied by an increase in the pressure drop [4-6]. Therefore, the main problem when designing VG-based heat exchangers is achieving a compromise between the heat exchange performance and hydraulic losses. Therefore, several geometrical factors have been extensively studied, including the angle of attack, height ratio, spacing, and arrangement of VGs [7-9].

Numerous types of VGs have been studied, such as delta winglets, rectangular winglets, trapezoidal configurations, and curved VGs. For instance, longitudinal VGs significantly improve the thermal conductivity by forming intense vortex flows inside the channel [10, 11]. Likewise, the rectangular winglet VG exhibited high thermo-hydraulic efficiency owing to its ability to create stable vortex structures [12]. Moreover, novel VG designs have recently been analyzed in numerical and experimental investigations of CHEs [13, 14].

In this context, the present study introduces a parametric investigation of VGs based on the edge number (N) as the primary geometric parameter. Block-type VG arrays with different polygonal cross-sections (triangular, square, pentagonal, hexagonal, and circular) were analyzed in a rectangular compact heat exchanger channel under a transitional-to-turbulent flow regime. This study aimed to establish a direct relationship between geometric complexity and thermo-hydraulic performance.

Despite extensive research on VGs, most studies are geometry-specific and do not provide a unified framework for comparing different configurations of VGs. In particular, the influence of the edge number as a systematic geometric parameter has not been sufficiently quantified under consistent constraints, limiting the identification of an optimal design.

To achieve this, three-dimensional Computational Fluid Dynamics (CFD) simulations were conducted to evaluate key performance parameters, including the Nusselt number (Nu), friction factor, and performance evaluation criterion (PEC). In addition, sophisticated analysis tools, such as entropy generation and field synergy, were employed to achieve a greater physical understanding of the fundamental heat transfer processes. Furthermore, a predictive model based on machine learning techniques was generated using the simulation dataset to calculate the performance-enhancing coefficient depending on the Reynolds number (Re) and edge number.

In addition to physics-based simulations, data-driven approaches have recently been used to analyze complicated interactions between thermofluid dynamics [13-15]. In this study, machine learning was used as an additional approach to explore the effects of the number of edges on thermo-hydraulic performance, rather than building a prediction model using machine learning. The uniqueness of this study lies in the inclusion of the edge number as one of the key parameters during the design process of such devices, along with the combination of physics-based and data-driven approaches. These findings will help establish design rules for next-generation VGs in heat-exchanger systems.

The specific contributions of this study are threefold:

1. Geometric Novelty: Introducing a systematic, edge-number-based parameterization method ($N = 3,4,5,6,\infty$) under fixed projected frontal area (A_p) and blockage ratio (BR) constraints to unify the evaluation of polygonal VGs.
2. Thermo-Physical Interpretation: Uncovering the structural role of geometry on the compromise between vortex strength (vorticity, ω) and flow dead-zones using field synergy angle (θ) and entropy generation (S_{gen}) principles.
3. Data-Driven Exploratory Role: Utilizing machine learning techniques not merely for interpolation, but as an advanced data-driven tool to confirm the continuity of performance trends and evaluate the joint dependency of PEC on the flow regime (Re) and geometric shape (N).

2. MATERIALS AND METHODS

2.1 Physical model and geometry

This study investigates the thermo-hydraulic performance of a rectangular compact heat exchanger channel equipped with block-type VG arrays mounted on a heated surface.

Table 1. Geometric dimensions of the computational domain for the rectangular compact heat exchanger channel

Parameter	Symbol	Value
Channel height	H	20 mm
Channel width	W	60 mm
Channel length	L	600 mm
Hydraulic diameter	D_h	Calculated

The computational domain represented a simplified segment of a compact heat exchanger to capture the essential flow and heat transfer characteristics. The channel dimensions were selected to ensure fully developed turbulent flow conditions, as summarized in Table 1.

The hydraulic diameter is defined as:

$$D_h = \frac{4A}{P} \tag{1}$$

where, D_h is the hydraulic diameter (m), A is the flow cross-sectional area (m²), and P is the wetted perimeter (m).

The computational domain and VG configurations are shown in Figure 1.

2.2 Vortex generator geometry

Five VG geometries were designed based on the number of edges (N), namely triangular (N = 3), square (N = 4), pentagonal (N = 5), hexagonal (N = 6), and circular (N = infinity) cross sections. All configurations were implemented as block-type VGs mounted on the heated wall of the channel. To ensure a consistent and fair comparison between different geometries, all the VGs were designed with identical projected frontal areas, heights, and attack angles. All VGs were systematically arranged at a fixed attack angle of alpha = 45° relative to the main fluid flow direction. Therefore, any variation in the thermo-hydraulic performance can be attributed primarily to differences in the geometric shape, particularly the edge number. The geometric characteristics of the investigated VG configurations are summarized in Table 2. All geometries were designed with an identical projected frontal area and BR to ensure a fair comparison, while only the edge number was varied.

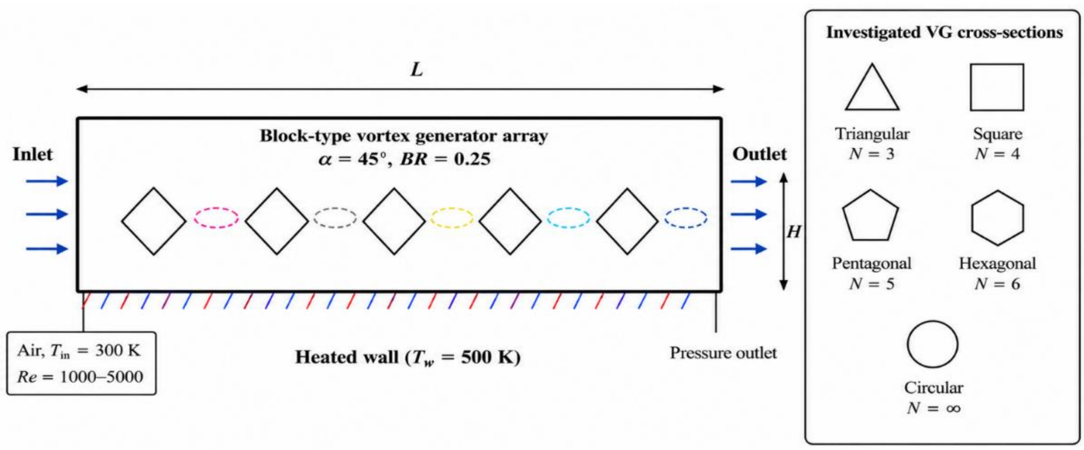

Figure 1. Schematic of the rectangular compact heat exchanger channel equipped with a block-type vortex generator (VG) array and investigated cross-sectional geometries

Table 2. Geometric parameters of the investigated vortex generator (VG) cross-sections under a constant projected frontal area

Shape	N	Projected Frontal Area (A_p) (mm²)	Perimeter (P) (mm)	Blockage Ratio (BR = b/H)
Triangle	3	25.00	22.80	0.25
Square	4	25.00	20.00	0.25
Pentagon	5	25.00	19.06	0.25
Hexagon	6	25.00	18.61	0.25
Circle	∞	25.00	17.72	0.25

Note: N = number of edges; namely triangular (N = 3), square (N = 4), pentagonal (N = 5), hexagonal (N = 6), and circular (N = infinity).

While maintaining the same projected surface area and obstruction ratio, the perimeter was allowed to change depending on the number of edges, thereby representing the variations in the geometric compactness of the shape. This variation can be better understood using a dimensionless shape factor, which is explained in Section 2.3.

2.3 Shape factor definition

To characterize the geometric influence of the VG cross-sections in a consistent and dimensionless manner, a shape factor based on geometric compactness was introduced [9].

The following definition was adopted.

$$\Phi_s = \frac{4\pi A_p}{P^2} \tag{2}$$

where,

A_p is the projected frontal area of the VG, and

P is the perimeter of the cross-section.

The resultant quantity provides a non-dimensional measure of shape compactness; as the value approaches one, the geometry is smoother (for instance, circular shapes), and as it falls below one, the shape is less smooth (triangular shapes, for instance). This method allows for a physical comparison between various shapes, regardless of their dimensions. In the present study, the projected frontal area was maintained constant for all geometries, and the shape factor was used to quantify the variations in the geometric complexity associated with the edge number.

2.4 Governing equations

The flow was modeled using Reynolds-averaged Navier–Stokes (RANS) equations [10]. Turbulent stresses were represented using an eddy viscosity approach based on the Boussinesq approximation. The energy equation includes a turbulent heat flux modeled using a turbulent Prandtl number.

2.5 Turbulence modeling

The flow regime spanned the transitional-to-turbulent range (Re = 1000 – 5000). Therefore, the SST–γ–Reθ transition model was employed as the primary model to capture the onset and development of the transition and improve near-wall accuracy [8].

For comparison at higher Re, the RNG k–ε model was also applied. The use of a transition-sensitive model enhances the reliability of these results.

2.6 Boundary conditions

The boundary conditions applied in the present simulations are listed in Table 3.

Table 3. Numerical and physical boundary conditions used in the baseline and enhanced channel Computational Fluid Dynamics (CFD) simulations

Parameter / Setup Component	Specifications / Values
Flow Regime (Re)	Working Fluid $1000 \le Re \le 5000$(Transitional-to-Turbulent)
Inlet Temperature (T_{in})	300 K
Inlet Boundary Condition	Uniform velocity based on target Reynolds number (Re)
Outlet Boundary Condition	Pressure outlet $\left(P_{gauge} = 0 \text{ Pa}\right)$
Wall Boundary Conditions	No-slip conditions on all solid boundaries
Heated Wall Condition	Constant heat flux (q") = 1000 W/m²
Turbulence Model	$SST - \gamma - Re_\theta$Transition Model (Primary); $RNGk - \varepsilon for\ high\ Re$ comparison
Near-Wall Treatment (y^+)	Strictly y+ < 1 across all solid boundaries
Mesh Type	Hybrid mesh with inflation layers and local refinement near VG edges
Discretization Scheme	Second-order upwind for momentum and energy equations
Pressure-Velocity Coupling	SIMPLE Algorithm
Convergence Criteria	Normalized residuals < 10^{-6} for all equations
Monitored Quantities	Area-weighted average temperature at outlet, total pressure drop (ΔP), and wall Nusselt number (Nu)

A constant heat flux boundary condition was imposed on the heated wall to better represent the practical compact heat exchanger operation and avoid inconsistencies associated with large temperature differences under constant wall temperature assumptions.

In addition, the thermophysical properties of air (density, viscosity, thermal conductivity, and specific heat) were treated as temperature-dependent and updated based on the local fluid temperature. This approach improves the physical realism of the simulation, particularly in nonuniform thermal conditions.

2.7 Reynolds number

The 'Reynolds number (Re)' is defined as

$$Re = \frac{\rho u D_h}{\mu} \tag{3}$$

where, u is the mean velocity (m/s).

The investigated range (Re = 1000 – 5000) covered the transitional-to-turbulent flow regime.

2.8 Mesh generation

A hybrid mesh was generated with local refinement near the VGs and inflation layers near the walls. To ensure the accuracy and reliability of the numerical results, a systematic mesh independence study was conducted using three distinct grid densities: coarse, medium, and fine. The variations in both the average Nusselt number (Nu) and the friction factor (f) were monitored at the highest flow velocity ($Re = 5000$) for the pentagonal configuration ($N = 5$), as summarized in Table 4.

Table 4. Multi-indicator grid convergence index and relative error analysis evaluated at Reynolds number (Re) = 5000 for the N = 5 geometry

Grid Level	Total Elements	Nusselt Number (Nu)	Relative Error (%)	Friction Factor (f)	Relative Error
Coarse	0.95×10^6	60.1	—	0.091	—
Medium (Accepted)	1.81×10^6	62.3	3.66%	0.085	6.59%
Fine	3.20×10^6	62.9	0.96%	0.084	1.18%

As detailed in the table, the relative errors for both Nu and f between the medium and fine meshes fell safely below 1.5%. Hence, the medium grid containing approximately 1.81 million cells was chosen for the remaining analysis to save computational cost. Also, a non-dimensional distance away from the wall $y^+ < 1$ was ensured to maintain near-wall accuracy.

2.9 Numerical solution

The governing equations were solved using the finite-volume method. The SIMPLE algorithm was used for pressure–velocity coupling, and second-order upwind schemes were applied. Convergence was achieved when residuals fell below 10^{-6}.

2.10 Model validation

A comprehensive validation procedure was conducted to ensure the reliability of the numerical model. First, a grid independence analysis was performed using three grids (coarse, medium, and fine) in the simulation. There was an error of less than 1.5% when comparing the Nusselt number (Nu) and pressure drop between the medium and fine grids, thus proving grid independence.

Second, the current numerical simulations of the smooth duct were compared with correlations from previous studies for turbulent flow in rectangular ducts, as quantitatively presented in Table 5. Good agreement was observed, with errors in the predictions not exceeding 5%. Furthermore, the numerical results were qualitatively compared with other studies involving CFD and experiments with VGs to enhance the performance of heat exchangers. Overall, this demonstrates that the numerical model provides reliable physical results within reasonable margins of error [3, 11].

2.11 Thermo-hydraulic performance evaluation framework

To establish a comprehensive thermal engineering assessment, evaluating a single parameter like the Nusselt number (Nu) is insufficient because it only quantifies convective heat transfer acceleration while ignoring pumping power penalties. Therefore, a multi-step sequential framework of performance indicators is implemented below to evaluate both the thermal gains and hydraulic costs.

2.11.1 Convective heat transfer characterization

The Nusselt number (Nu) represents the ratio between convective and conductive heat transfers, providing a direct measure of the heat transfer enhancement owing to vortex-induced mixing. A higher Nu value is always desirable for accelerated thermal dissipation:

- Nusselt number (Nu):

$$Nu = \frac{hD_h}{k} \tag{4}$$

where, h is the convective heat transfer coefficient (W/m²·K), D_h is the hydraulic diameter (m), and k is the thermal conductivity of the fluid (W/m·K).

2.11.2 Hydraulic resistance assessment

The friction factor (f) reflects the aerodynamic or hydraulic resistance imposed by the VGs, which is primarily associated with the form drag and flow separation. A lower friction factor is desired to minimize the required pumping power.

- Friction factor (f):

$$f = \frac{\Delta P}{(L/D_h)(\rho u^2/2)} \tag{5}$$

where, ΔP is the pressure drop (Pa), L is the channel length (m), ρ is the fluid density (kg/m³), and u is the mean velocity (m/s).

2.11.3 Comprehensive optimization (performance evaluation criterion analysis)

The PEC provides a balanced evaluation by comparing the relative increase in heat transfer with the associated increase in the pressure drop under equal pumping power constraints. A PEC value greater than unity (PEC > 1) confirms a net thermo-hydraulic benefit.

- PEC:

$$PEC = \frac{Nu/Nu_0}{(f/f_0)^{1/3}} \tag{6}$$

where, Nu_0 and f_0 correspond to the smooth channel (baseline case). PEC is 'PEC'.

Table 5. Quantitative baseline validation benchmarking smooth duct numerical predictions against classic empirical correlations

Reynolds Number (Re)	Present CFD (Nu_0)	Dittus-Boelter (Nu)	Deviation (%)	Present CFD (f_0)	Petukhov (f)	Deviation (%)
1000	12.5	11.9	+5.04%	0.082	0.079	+3.80%
3000	23.6	24.4	−3.28%	0.064	0.061	+4.92%
5000	34.1	35.2	−3.12%	0.053	0.051	+3.92%

Note: Computational Fluid Dynamics (CFD).

2.12 Advanced analysis

Additional flow characteristics were evaluated using the following:

- Vorticity:

$$\omega = \nabla \times \vec{u} \quad (7)$$

where,
ω is the vorticity (1/s), and
$\vec{u}$ is the velocity vector.
Vorticity represents the local rotational motion of a fluid and is used to characterize the vortex strength.

- Entropy generation:

$$S_{gen} = S_{thermal} + S_{friction} \quad (8)$$

where, $S_{thermal}$ is the entropy generation due to heat transfer, and $S_{friction}$ is the entropy generation due to viscous effects.
This parameter reflects the thermodynamic irreversibility within the system.

- Field synergy angle:

$$\theta = \angle(\vec{u}, \nabla T) \quad (9)$$

where, θ represents the angle between the velocity vector and the temperature gradient vector. The smaller the value of θ, the closer the alignment of the two vectors, leading to better convective heat transfer performance.

2.13 Machine learning model

In order to evaluate the correlation between Re, edge number, and PEC, a machine learning model was formulated. Due to the small amount of data available for analysis, the model could only be used in an exploratory role rather than a purely predictive one [16-18]. Model performance was evaluated using various cross-validation methods.

3. RESULTS

3.1 Heat transfer performance (Nusselt number)

The variation in the average Nusselt number (Nu) with the Re is presented in Table 6 and illustrated in Figure 2.
The results show that Nu increases with the Re for all configurations. Compared with the smooth channel, all the VG cases exhibited enhanced heat transfer.
Among the geometries investigated, the pentagonal configuration (N = 5) consistently provided the highest Nusselt number (Nu). At Re = 5000, Nu increases from 34.1 for the smooth channel to 62.3 for N = 5.

3.2 Friction factor

The friction factor values are listed in Table 7 and are plotted in Figure 3.
The results indicate that the friction factor decreased with increasing Re for all cases. However, all the VG configurations produced higher pressure losses than the baseline case.
The triangular geometry (N = 3) exhibited the highest friction factor, whereas the circular configuration (N = ∞) exhibited the lowest values among the VG cases.

Table 6. Variation of the average Nusselt number (Nu) with Reynolds number (Re) for different vortex generator (VG) edge numbers

Re	No VG	N = 3 (Tri)	N = 4 (Square)	N = 5 (Pentagon)	N = 6 (Hexagon)	N = ∞ (Circle)
1000	12.5	18.9	20.8	22.6	21.5	19.7
2000	18.2	27.5	30.1	32.8	31.0	28.9
3000	23.6	35.8	39.2	42.5	40.1	37.6
4000	28.9	44.2	48.5	52.4	49.8	46.3
5000	34.1	52.7	57.9	62.3	59.2	55.1

Table 7. Variation of the friction factor with Reynolds number (Re) for different vortex generator (VG) edge numbers

Re	No VG	N = 3	N = 4	N = 5	N = 6	N = ∞
1000	0.082	0.141	0.132	0.125	0.121	0.115
2000	0.071	0.124	0.117	0.110	0.106	0.101
3000	0.064	0.112	0.105	0.099	0.096	0.092
4000	0.058	0.103	0.097	0.092	0.089	0.086
5000	0.053	0.095	0.090	0.085	0.083	0.080

3.3 Performance evaluation criterion

The PEC are presented in Table 8 and Figure 4.
The results indicate that all PEC values exceed unity, thereby confirming the effectiveness of the VGs. The pentagonal configuration (N = 5) exhibited the highest performance across all Re.
Specifically, when Re = 5000, the performance criterion equals about 1.56, whereas for N = 3 the decrease is noted at higher Re.

Table 8. Performance evaluation criterion (PEC) calculated for different vortex generator (VG) edge numbers over the investigated Reynolds number (Re) range

Re	N = 3 (Tri)	N = 4 (Square)	N = 5 (Pentagon)	N = 6 (Hexagon)	N = ∞ (Circle)
1000	1.26	1.42	1.54	1.48	1.40
2000	1.25	1.41	1.55	1.49	1.41
3000	1.25	1.42	1.56	1.50	1.42
4000	1.26	1.42	1.56	1.50	1.42
5000	1.27	1.42	1.56	1.51	1.41

3.4 Entropy generation

The entropy generation results are summarized in Table 9 and shown in Figure 5.
As the Re increased, the entropy generation increased in all cases. The entropy generated was minimum in the case of the pentagonal shape (N = 5).

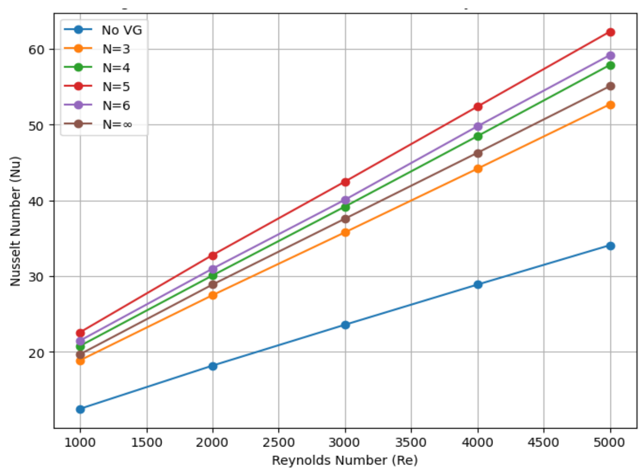

Figure 2. Variation of average Nusselt number (Nu) with Reynolds number (Re) (1000 <= Re <= 5000) for five block-type vortex generator (VG) geometries (N = 3 to infinity) compared against the smooth channel baseline under constant wall heat flux conditions

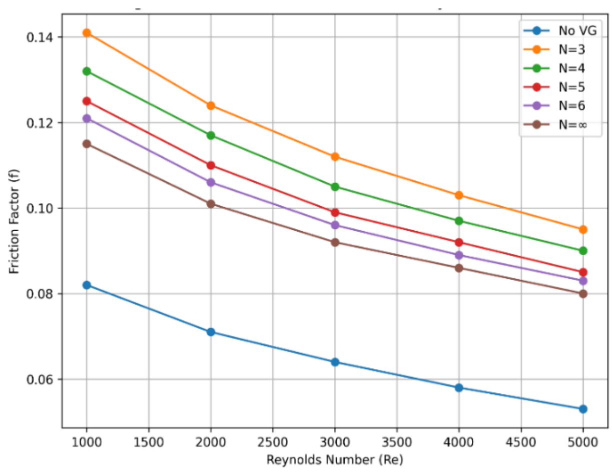

Figure 3. Dependence of the fluid friction factor (f) on the Reynolds number (Re) span for various polygonal vortex generator (VG) configurations and the baseline smooth channel assembly

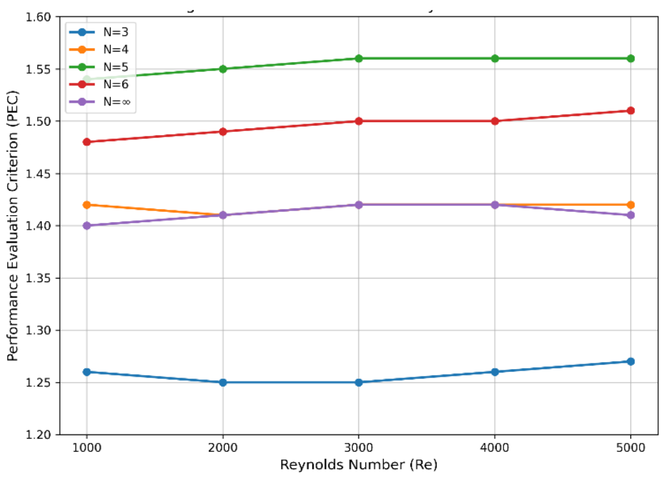

Figure 4. Variation of the overall performance evaluation criterion (PEC) as a function of Reynolds number (Re), highlighting the net thermo-hydraulic efficiency threshold across different geometric edge numbers

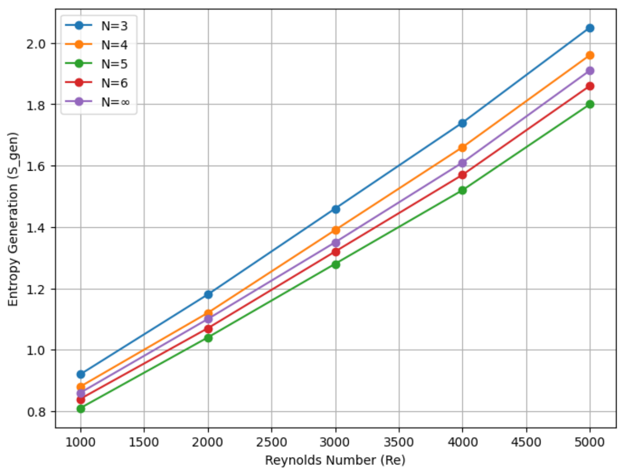

Figure 5. Total entropy generation (S_{gen}) rates plotted against Reynolds number (Re) to evaluate the thermodynamic irreversibility metrics for each vortex generator (VG) configuration

Table 9. Total entropy generation for different vortex generator (VG) geometries as a function of Reynolds number (Re)

Re	N = 3	N = 4	N = 5	N = 6	N = ∞
1000	0.92	0.88	0.81	0.84	0.86
2000	1.18	1.12	1.04	1.07	1.10
3000	1.46	1.39	1.28	1.32	1.35
4000	1.74	1.66	1.52	1.57	1.61
5000	2.05	1.96	1.80	1.86	1.91

Table 10. Maximum vorticity values obtained for different vortex generator (VG) edge numbers under various Reynolds numbers (Re)

Re	N = 3	N = 4	N = 5	N = 6	N = ∞
1000	320	295	275	250	210
2000	520	485	455	420	360
3000	720	670	630	580	510
4000	910	860	810	750	660
5000	1100	1040	980	910	800

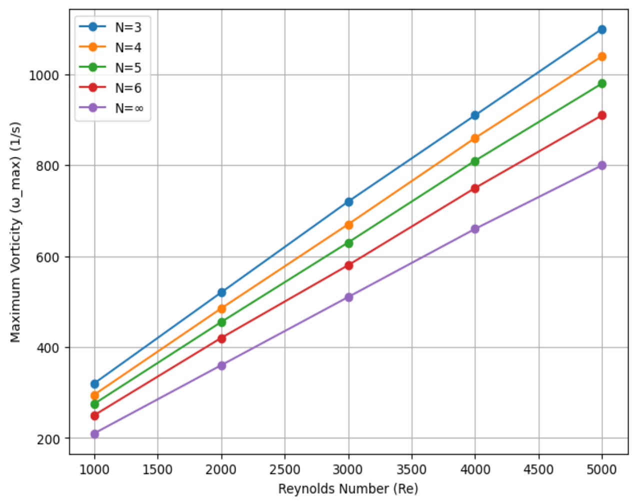

Figure 6. Distribution of peak vorticity magnitudes (ω_{max}) across the investigated transitional-turbulent velocity range for the different geometric cross-sections

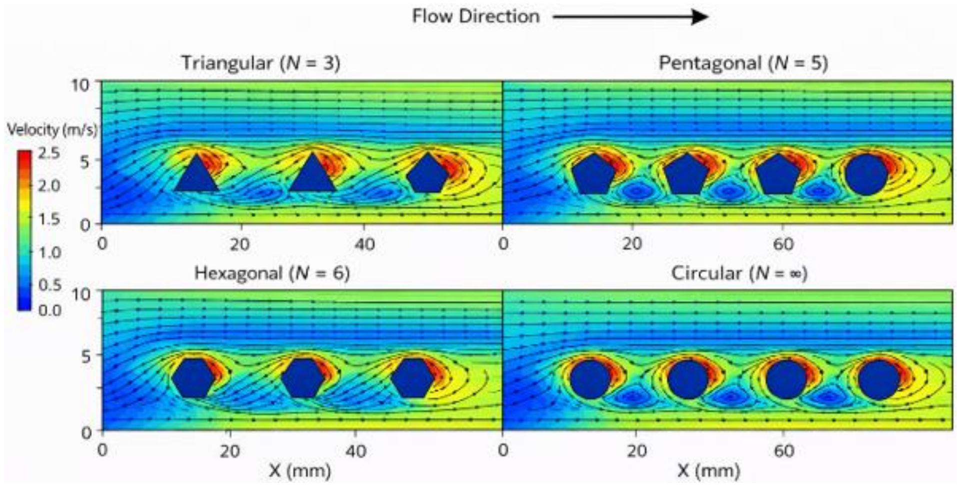

Figure 7. Two-dimensional mid-plane velocity streamlines and core flow structures plotted for targeted vortex generator (VG) configurations: (a) Triangular (N = 3), (b) Pentagonal (N = 5), (c) Hexagonal (N = 6), and (d) Circular (N = infinity) at Re = 5000

Table 11. Mean field synergy angle (θ) variations in degrees across the investigated Reynolds number (Re)

Re	N = 3	N = 4	N = 5	N = 6	N = ∞
1000	42.1	39.5	36.8	38.2	40.1
2000	40.3	37.8	35.2	36.7	38.5
3000	38.9	36.2	33.8	35.4	37.1
4000	37.5	34.9	32.6	34.1	35.9
5000	36.2	33.5	31.4	33.0	34.8

3.5 Vorticity distribution

The maximum vorticity values are listed in Table 10 and are presented in Figure 6.

Figure 7 presents the streamlines for different geometries of VGs, depending on the number of edges of the VG.

From the analysis, the triangular pattern (N = 3) exhibited the highest vorticity values. The vorticity decreased with an increase in the number of edges, and the minimum vorticity values were obtained for the circular shape.

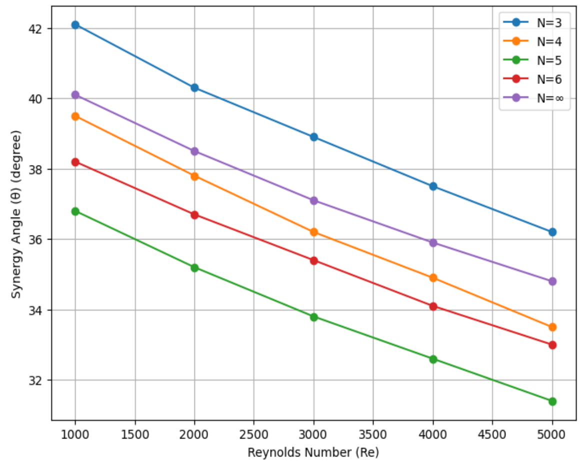

Figure 8. Evaluated mean field synergy angle (θ) variations across the dynamic flow range, indicating the structural vector alignment between fluid velocity and localized temperature gradients

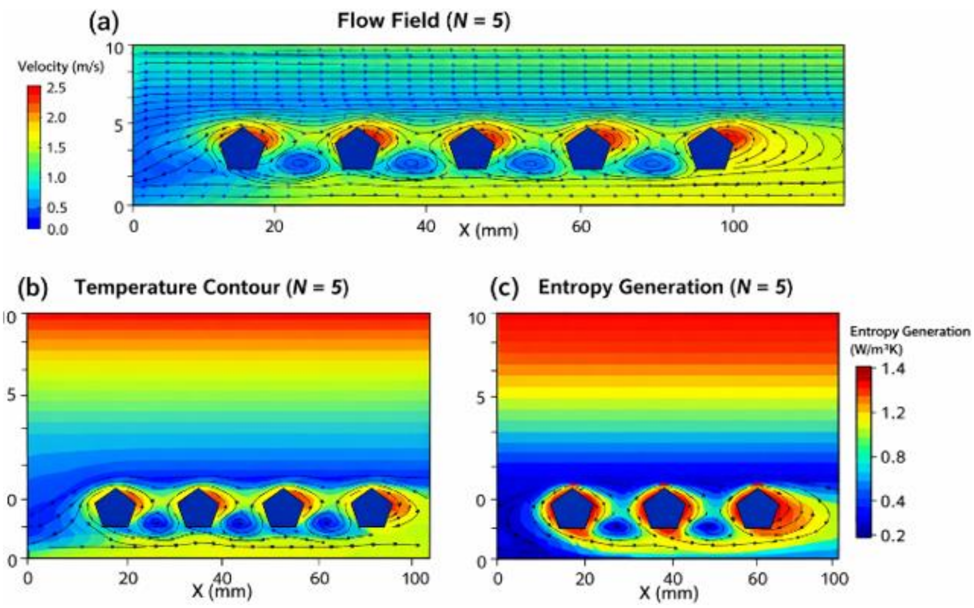

Figure 9. High-fidelity localized numerical field representations for the optimal pentagonal design (N = 5): (a) absolute velocity streamlines, (b) temperature field contours detailing thermal boundary layer thinning, and (c) volumetric entropy generation profiles identifying primary dissipation regions

3.6 Field synergy angle

The field synergy angle is listed in Table 11 and plotted in Figure 8.

As the Reynolds number (Re) increased, the synergy angle decreased. The minimum synergy angles were found in the case of the pentagonal shape (N = 5).

The flow and thermal fields for N = 5 are shown in Figure 9.

Table 12. Structured high-fidelity CFD dataset constructed for training and mapping within the exploratory surrogate machine learning framework

Re	N	/1N	Nu	f	PEC
1000	3	0.333	18.9	0.141	1.26
1000	4	0.250	20.8	0.132	1.42
1000	5	0.200	22.6	0.125	1.54
1000	6	0.167	21.5	0.121	1.48
1000	∞	0.000	19.7	0.115	1.40
2000	3	0.333	27.5	0.124	1.25
2000	4	0.250	30.1	0.117	1.41
2000	5	0.200	32.8	0.110	1.55
2000	6	0.167	31.0	0.106	1.49
2000	∞	0.000	28.9	0.101	1.41
3000	3	0.333	35.8	0.112	1.25
3000	4	0.250	39.2	0.105	1.42
3000	5	0.200	42.5	0.099	1.56
3000	6	0.167	40.1	0.096	1.50
3000	∞	0.000	37.6	0.092	1.42
4000	3	0.333	44.2	0.103	1.26
4000	4	0.250	48.5	0.097	1.42
4000	5	0.200	52.4	0.092	1.56
4000	6	0.167	49.8	0.089	1.50
4000	∞	0.000	46.3	0.086	1.42
5000	3	0.333	52.7	0.095	1.27
5000	4	0.250	57.9	0.090	1.42
5000	5	0.200	62.3	0.085	1.56
5000	6	0.167	59.2	0.083	1.51
5000	∞	0.000	55.1	0.080	1.41

Note: Computational Fluid Dynamics (CFD), Reynolds number (Re), edge number (N), inverse edge number (1/N), Nusselt number (Nu), friction factor (f), and performance evaluation criterion (PEC) were used as the primary dataset features.

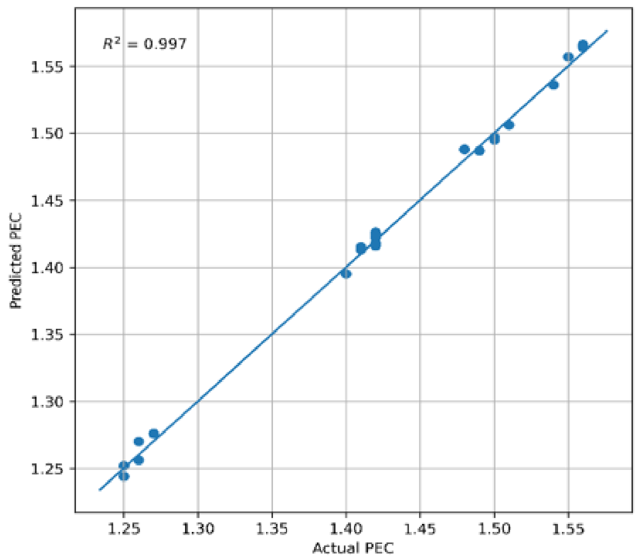

Figure 10. Parity plot demonstrating actual Computational Fluid Dynamics (CFD)-derived performance evaluation criteria (PEC) values versus predictions computed via the data-driven exploratory surrogate mode

3.7 Machine learning results

The complete dataset used for the exploratory machine learning analysis is presented in Table 12. The input features included the Re and edge number, whereas the output target was the PEC.

The PEC trend in the current data is consistent with that seen in the previous numerical analysis, in which the PEC was highest for the pentagonal geometry, while frictional losses were maximum in the case of the triangular geometry.

A comparison between the predicted and numerical PEC values is shown in Figure 10.

There is a close correlation between the PEC values predicted by the theory and numerical calculations.

4. DISCUSSION

4.1 Effect of edge number on heat transfer enhancement

The findings show a marked increase in the Nusselt number (Nu) due to the presence of VGs, where the highest values are recorded for N = 5. The reason for such an increase is due to the formation of longitudinal vortices that cause better mixing of the fluids and a reduction in the thermal boundary layer. From previous research, it has been proven that VGs cause a secondary flow that brings fluids with high momentum closer to the wall that is heated [19-21]. This process increases the possibility of heat energy transfer from the core to the near-wall region, resulting in a higher heat transfer coefficient. The superior performance of the pentagonal shape indicates that vortex strength alone cannot explain the increased heat transfer; the spatial and temporal distributions of the vortex structures can also play a role in determining the effect. As shown in the dynamic contours of Figures 7 and 9, the pentagonal shape generates well-structured longitudinal vortices that facilitate effective fluid mixing and systematic thinning of the thermal boundary layer. Higher heat transfer was also evident near the heated wall from the temperature profiles, and the entropy distribution revealed less thermodynamic irreversibility than that of the other shapes. This kind of physical behavior makes it easy to trace the direct link between geometry and macro performance. Geometries with sharp profiles, such as the N = 3 triangular case, generate rapid flow separation and create high peak vorticity values. The velocity streamlines presented across the comparative channels in Figure 7 confirm the presence of large zones of low-velocity recirculations formed by such sharp edges. The lack of mixing of heat through the core flow due to such zones leads to thermal choking and high drag losses, contributing to a lower overall PEC value.

Conversely, the intermediate pentagonal cross-section (N = 5) provides a managed flow detachment profile. It creates strong, well-structured longitudinal vortices that successfully sweep high-momentum core fluid toward the heated wall, continuously disrupting and thinning the thermal boundary layer. This effective fluid mixing occurs with minimal aerodynamic energy dissipation, seamlessly bridging the gap between localized vortex physics and global heat transfer magnification.

4.2 Influence of geometry on vortex structure

Based on the vorticity results, it is clear that the triangular configuration (N = 3) provides the highest peak vorticity values. Sharp geometries create flow separation conditions that help initiate vortex formation [22]. However, a high peak vorticity does not imply good thermal performance. As stated above, effective mixing of fluid flow is one of the key factors that contribute to enhanced heat transfer, whereas excessive flow separation might lead to the appearance of dead zones and insufficient mixing of the flow [23]. In this regard, geometries that produce effective vortical structures with the least flow separation help achieve the best performance.

4.3 Pressure drop characteristics

The results for the friction factor showed that all configurations with VGs significantly increased the flow resistance compared to the smooth channel owing to the induced flow disruption and turbulence. Such behavior is typical for VG configurations because improvements in thermal performance are usually achieved at the expense of higher pressure losses [24-26]. The triangular geometry results in higher friction factor values because of its strong effect on the fluid flow and flow separation. Smoother geometries, such as circular ones, provide low-pressure losses owing to reduced flow separation, although the increase in heat transfer performance is not significant.

4.4 Thermo-hydraulic performance (performance evaluation criterion analysis)

The PEC results revealed that the pentagonal geometry exhibited the highest performance value. PEC can be used to evaluate the thermo-hydraulic performance of configurations by considering the contribution of thermal and hydraulic phenomena [27, 28]. For efficient configurations, the relative increase in heat transfer should exceed the relative increase in the pressure losses. It should be stressed that the presented results represent an optimal combination of thermal and hydraulic performance under the given geometric and flow conditions.

4.5 Entropy generation analysis

The entropy generation results showed that the pentagonal geometry resulted in the lowest values. Entropy generation can be used as a measure of the thermodynamic irreversibility that occurs during heat transfer and viscous dissipation [29]. Thus, lower entropy generation corresponds to a higher energy efficiency. As can be seen, the pentagonal geometry (N = 5) achieves low entropy generation values, indicating that such a configuration helps minimize thermodynamic irreversibility.

This thermo-physical causal chain is strongly validated by the second-law thermodynamic assessments and the field synergy principle. The pentagonal geometry (N = 5) minimizes thermodynamic irreversibilities, yielding the lowest total entropy generation (S_{gen} = 1.80 W/K at Re = 5000). This optimization is driven by achieving the lowest field synergy angle (theta = 31.4 degrees at Re = 5000), indicating that the local fluid velocity vectors are structurally aligned with the temperature gradients. This superior coordination ensures that convective heat transfer is accelerated while hydrodynamic friction expenditures are minimized, proving that the pentagonal design is highly justified for industrial deployment.

4.6 Field synergy principle

The analysis of the angle between the velocity vector and temperature gradient showed that the synergy angle was minimal for the pentagonal geometry. According to the field synergy principle, heat transfer increases with a decrease in the angle between the temperature gradient and fluid flow direction [30]. As shown, the configuration that provides the smallest synergy angle (N = 5) is characterized by the highest heat transfer values.

4.7 Machine learning interpretation

According to the results obtained using machine learning techniques, the dependence between the Re, edge number, and PEC can be described using data-driven modeling. Recent studies have shown that machine learning techniques can successfully predict the properties of thermo-fluid systems and uncover the relationship between geometric and operating parameters [16, 18]. In this study, the formulated data-driven architecture operates strictly as a CFD-based exploratory surrogate model intended for rapid parameter mapping. Given that it is trained on a localized numerical dataset, it serves an exploratory role to smoothly trace performance tendencies across continuous variables. Consequently, this surrogate model must not be extrapolated outside the strictly verified bounds of this study, namely the Re interval of 1000 to 5000 and the investigated polygonal geometries (N = 3 to 6, and infinity).

4.8 Limitations and perspectives

This study had several limitations. However, it should be noted that this is based only on simulation results, and further verification of the findings with experimental data is necessary. In addition, the analysis of VG geometries was performed under fixed parameters of spacing, arrangement, and angle; therefore, changes in these factors might affect the performance. In addition, this study focused only on the heat transfer of single-phase airflow under certain conditions. Moreover, the range of Re (1000-5000) represents the transitional-turbulent regime.

Future studies should focus on experimental validation, geometric optimization, and integration of advanced data-driven models using larger datasets.

It must be emphasized that because the data-driven model is trained exclusively on the high-fidelity CFD dataset, it operates strictly as a fast surrogate screening tool within the studied parameter constraints. The model represents an interpolation framework intended for rapid design mapping of geometric edge numbers and flow conditions; it should not be extrapolated to untested geometric profiles or Re envelopes outside the verified bounds of 1000 to 5000, where different boundary layer transition physics may dominate.

5. CONCLUSIONS

Based on the numerical and data-driven investigation of block-type VGs in a compact heat exchanger channel, several key conclusions can be drawn regarding the structural role of geometry. The parametric analysis demonstrates that geometric modifications driven by the edge number affect thermal and hydraulic performance differently. While all configurations successfully augment the heat transfer rate relative to the smooth channel baseline, this thermal acceleration is continuously accompanied by an increased pressure drop penalty. Therefore, evaluating the thermal enhancement alone is insufficient without accounting for the associated flow resistance and pressure penalties. Across the entire transitional-to-turbulent flow span, the performance analysis indicates that an intermediate geometry yields the most effective balance of properties, with the pentagonal configuration (N = 5) representing the optimal design that achieves the maximum PEC of approximately 1.56 at Re = 5000. Furthermore, second-law thermodynamic assessments and the field synergy principle confirm that this optimal pentagonal geometry provides the lowest thermodynamic irreversibility, minimizing entropy generation while achieving superior structural coordination between the flow velocity vectors and local temperature gradients. In parallel, the exploratory machine learning analysis successfully captures and reproduces the prominent performance and geometric tendencies established by the high-fidelity CFD model, demonstrating that data-driven approaches can be reliably exploited to screen design tendencies within defined operational bounds. Ultimately, the obtained data provide essential design insights for implementing advanced VGs in compact thermal systems. However, these quantitative findings remain strictly valid for the selected physical envelopes, including the specific attack angle of 45 degrees, the particular VG arrangement, and the investigated transitional-turbulent Re interval.

REFERENCES

[1] Fiebig, M. (1995). Vortex generators for compact heat exchangers. Journal of Enhanced Heat Transfer, 2(4): 295-305. https://doi.org/10.1615/JEnhHeatTransf.v2.i4.50

[2] Bashtani, I., Abolfazli Esfahani, J. (2025). Predicting the physics of turbulent fluid flow passing through nature-inspired dolphin turbulator by artificial neural network. Journal of Thermal Analysis and Calorimetry, 150(11): 8289-8306. https://doi.org/10.1007/s10973-024-13561-2

[3] Kareem, D.F., Mohammed, A.A., Al-Gburi, H. (2023). Empirical investigation of thermal features of phase change material as thermal storage system. Journal of Advanced Research in Fluid Mechanics and Thermal Sciences, 111(2): 154-169. https://doi.org/10.37934/arfmts.111.2.154169

[4] He, Y.L., Han, H., Tao, W.Q., Zhang, Y.W. (2012). Numerical study of heat-transfer enhancement by punched winglet-type vortex generator arrays in fin-and-tube heat exchangers. International Journal of Heat and Mass Transfer, 55(21-22): 5449-5458. https://doi.org/10.1016/j.ijheatmasstransfer.2012.04.059

[5] Luo, Y., Li, G., Bennett, N.S., Luo, Z., Munir, A., Islam, M.S. (2025). Heat transfer enhancement in heat exchangers by longitudinal vortex generators: A review of numerical and experimental approaches. Energies, 18(11): 2896. https://doi.org/10.3390/en18112896

[6] Feng, Z., Jiang, P., Zheng, S., et al. (2023). Experimental and numerical investigations on the effects of insertion-type longitudinal vortex generators on flow and heat transfer characteristics in square minichannels. Energy, 278: 127855. https://doi.org/10.1016/j.energy.2023.127855

[7] Batista, J., Trp, A., Lenic, K., Kirincic, M. (2025). The influence of geometry parameters of rectangular vortex generators on the air-to-water fin-and-tube heat exchanger efficiency enhancement. International Communications in heat and mass transfer, 162: 108647. https://doi.org/10.1016/j.icheatmasstransfer.2025.108647

[8] Tanougast, A., Hriczó, K. (2025). Enhanced heat transfer in wavy channels with vortex generators: A CFD investigation. International Journal of Thermofluids, 30, 101405. https://doi.org/10.1016/j.ijft.2025.101405

[9] Liang, X., Min, M., Bian, K., Cheng, J. (2025). Study on the enhanced heat transfer and exergy performance of the finned tube heat exchanger with vortex generator. International Journal of Thermal Sciences, 210: 109639. https://doi.org/10.1016/j.ijthermalsci.2024.109639

[10] Ahmadi, N., Rostami, S., Damya, A. (2025). Smart design of conical vortex generators for heat transfer enhancement: A synergy of CFD and Bio-inspired optimization. Results in Engineering, 27: 105613. https://doi.org/10.1016/j.rineng.2025.105613

[11] Bahuguna, R., Mer, K.K.S., Kumar, M., Chamoli, S. (2025). Entropy generation analysis in a tube heat exchanger integrated with triple blade vortex generator inserts. Energy Sources, Part A: Recovery, Utilization, and Environmental Effects, 47(1): 7264-7282. https://doi.org/10.1080/15567036.2021.1918291

[12] Guo, Z.Y., Li, D.Y., Wang, B.X. (1998). A novel concept for convective heat transfer enhancement. International Journal of Heat and Mass Transfer, 41(14): 2221-2225. https://doi.org/10.1016/S0017-9310(97)00272-X

[13] Hussain, M., Lin, D., Waqas, H., Al-Mdallal, Q.M. (2025). An artificial intelligence and machine learning-driven CFD simulation for optimizing thermal performance of blood-integrated ternary nano-fluid. Engineering Applications of Computational Fluid Mechanics, 19(1): 2459664. https://doi.org/10.1080/19942060.2025.2459664

[14] Portal-Porras, K., Fernandez-Gamiz, U., Zulueta, E., Garcia-Fernandez, R., Irigaray, O. (2023). Parametric study of vortex generators on a fin-and-tube heat exchanger. Energy Sources, Part A: Recovery, Utilization, and Environmental Effects, 45(4): 10051-10072. https://doi.org/10.1080/15567036.2023.2242809

[15] Modi, A.J., Rathod, M.K. (2022). Experimental investigation of heat transfer enhancement and pressure drop of fin-and-circular tube heat exchangers with modified rectangular winglet vortex generator. International Journal of Heat and Mass Transfer, 189: 122742. https://doi.org/10.1016/j.ijheatmasstransfer.2022.122742

[16] Hughes, M.T., Kini, G., Garimella, S. (2021). Status, challenges, and potential for machine learning in understanding and applying heat transfer phenomena. Journal of Heat Transfer, 143(12): 120802. https://doi.org/10.1115/1.4052510

[17] Sulaiman, M., Khalaf, O.I., Khan, N.A., Alshammari, F.S., Algburi, S., Hamam, H. (2024). Machine learning-based prediction of heat transfer performance in annular fins with functionally graded materials. Scientific Reports, 14(1): 8801. https://doi.org/10.1038/s41598-024-58595-6

[18] Zobeiry, N., Humfeld, K.D. (2021). A physics-informed machine learning approach for solving heat transfer equation in advanced manufacturing and engineering applications. Engineering Applications of Artificial Intelligence, 101: 104232. https://doi.org/10.1016/j.engappai.2021.104232

[19] Al-Obaidi, A.R. (2024). Analysis of thermo-hydraulic flow and optimisation heat augmentation in 3D dimpled pipe based on design of experiment method and Taguchi technique evaluation. International Journal of Ambient Energy, 45(1): 2378951. https://doi.org/10.1080/01430750.2024.2378951

[20] Jasiński, P.B., Górecki, G., Cebulski, Z. (2024). Evaluation of the efficiency of heat exchanger channels with different flow turbulence methods using the entropy generation minimization criterion. Energies, 18(1): 132. https://doi.org/10.3390/en18010132

[21] Ifraj, N.F., Akter, F., Fahad, M.K., Ahmed, D.H. (2025). Thermal-hydraulic performance enhancement with minimum entropy generation of a heat exchanger using fidget spinner vortex generators. International Communications in Heat and Mass Transfer, 162: 108610. https://doi.org/10.1016/j.icheatmasstransfer.2025.108610

[22] Li, J., Ling, X., Peng, H. (2013). Field synergy analysis on convective heat transfer and fluid flow of a novel triangular perforated fin. International Journal of Heat and Mass Transfer, 64: 526-535. https://doi.org/10.1016/j.ijheatmasstransfer.2013.04.039

[23] Far, Z., Hekmat, M.H., Izadpanah, E. (2022). Vortex-induced vibration effects on mixing performance. Chemical Engineering and Processing-Process Intensification, 182: 109211. https://doi.org/10.1016/j.cep.2022.109211

[24] Ali, S., Dbouk, T., Wang, G., Wang, D., Drikakis, D. (2023). Advancing thermal performance through vortex generators morphing. Scientific Reports, 13(1): 368. https://doi.org/10.1038/s41598-022-25516-4

[25] Tian, Z., Zhang, Y., Xiong, X., Gou, G., Wu, Y. (2024). Performance enhancement of high temperature fin-and-tube heat exchanger employing winglet combined vortex generators. Applied Thermal Engineering, 249: 123376. https://doi.org/10.1016/j.applthermaleng.2024.123376

[26] Abbas, A.S., Mohammed, A.A. (2023). Enhancement of plate-fin heat exchanger performance with aid of (RWP) vortex generator. International Journal of Heat and Technology, 41(3): 780-788. https://doi.org/10.18280/ijht.410336

[27] Abbas, A.S., Mohammed, A.A. (2022). Augmentation of plate-fin heat exchanger performance with support of various types of fin configurations. Mathematical Modelling of Engineering Problems, 9(5): 1406-1414. https://doi.org/10.18280/mmep.090532

[28] Abbas, A.S., Mohammed, A.A. (2023). Improvement of plate-fin heat exchanger performance with assistance of various types of vortex generator. CFD Letters, 15(7): 131-147. https://doi.org/10.37934/cfdl.15.7.131147

[29] Feng, Z., Zhang, Q., Liang, S., et al. (2024). Hydrothermal, entropy generation and exergy performances analysis in a mini-channel with combination of longitudinal and transverse vortex generators using Al2O3 nanofluids. Powder Technology, 432: 119100. https://doi.org/10.1016/j.powtec.2023.119100

[30] Qi, X., Yang, J., Zhang, Y., Wang, J., Guo, X. (2025). Simulation study of the influence of circular arc vortex generator size on the heat transfer characteristics of fin-and-tube heat exchanger. Scientific Reports, 15(1): 22059. https://doi.org/10.1038/s41598-025-05071-4

NOMENCLATURE

A	Cross-sectional area
A_p	Projected frontal area of vortex generator
D_h	Hydraulic diameter
f	Friction factor
h	Convective heat transfer coefficient
k	Thermal conductivity
L	Channel length
N	Number of vortex generator edges
Nu	Nusselt number
P	Perimeter of vortex generator cross-section
PEC	Performance evaluation criterion
Re	Reynolds number
S_{gen}	Entropy generation
T	Temperature
u	Velocity magnitude

Greek symbols

α	Vortex generator attack angle
θ	Mean field synergy angle
μ	Dynamic viscosity
ρ	Fluid density
ω	Vorticity magnitude

Subscripts

h	Hydraulic
gen	Generation
max	Maximum value
f	Fluid property
th	Thermal enhancement component